

# A Multi-scale Study of the 23 October 2022 Southern England QLCS

**Kenneth Pryor, David Smart, David Flack, Matthew Clark**

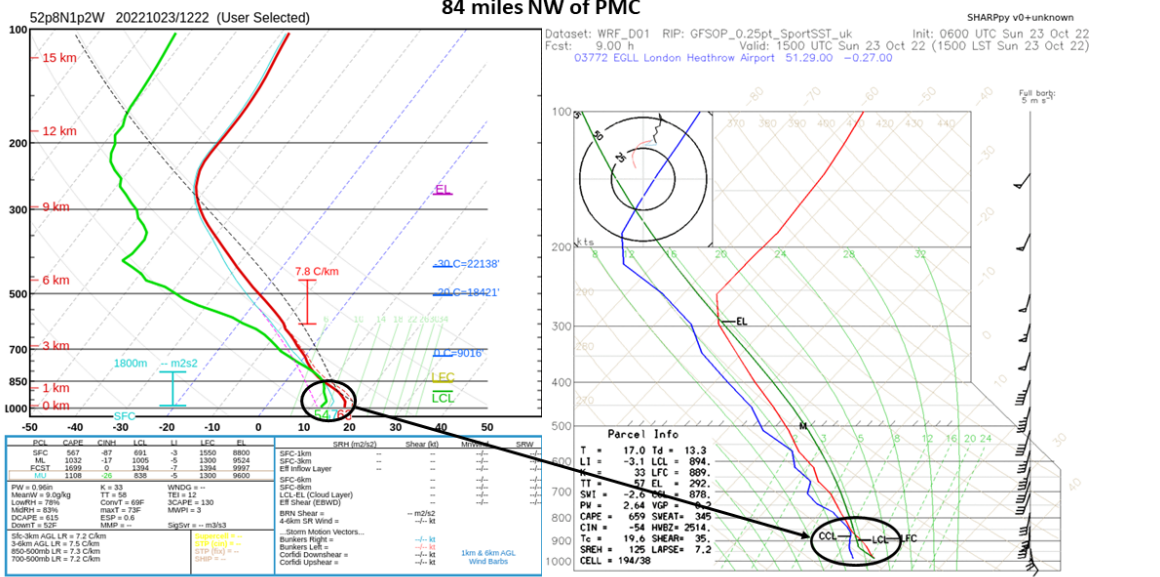
## Abstract

During the afternoon of 23 October 2022, a quasi-linear convective system (QLCS) developed and intensified over the English Channel and tracked north-northeastward into southern England, producing widespread damaging downburst winds. The highest measured downburst wind gusts of the event occurred at 1) Army Aviation Centre (AAC) Middle Wallop, Hampshire (55 miles SW of London), with a wind gust of 54 kt (62 mph) recorded between 1500 and 1600 UTC and generated by a prominent bowing segment of the QLCS; 2) London Colney, Hertfordshire, with a wind gust of 56 kt (64 mph) recorded at 1640 UTC and generated by a pulse-severe cell east of the bowing segment of the QLCS. In general, as shown in Figure 1, the early afternoon (1222 UTC) NOAA-20 NUCAPS sounding qualitatively indicated the strongest signal for severe thunderstorm and downburst occurrence over southern England:

1. It resolved a shallow elevated mixed layer detected by the closest downstream RAOB sounding at Nottingham.
2. Indicated more significant lower-middle tropospheric temperature lapse rates and CAPE than the adjacent AIRS sounding.
3. NUCAPS surface temperature (66°F/18°C) matched the temperature recorded at Herstmonceux, the closest observing station to the retrieval.

Mapped SSMIS imagery with UKMO rain radar overlays (see Figure 2) and a mid-day NUCAPS sounding profile over Leicestershire (~90 miles NW of London) provided the strongest signal for severe downburst winds in the pre-storm environment over the Midlands. Close agreement is noted between the boundary layer structure ("inverted-V") as resolved by the NUCAPS soundings and WRF profiles and the microburst windspeed potential index (MWPI) gust potential calculated from NUCAPS and the WRF model. A strong relationship between high rain rates, as indicated by UKMO radar, and the very low MW brightness temperatures (BTs) is apparent in both the consecutive F-18 and F-16 overpasses. Low BTs also correspond well with the high integrated graupel values, suggesting that intense downdrafts and resulting downbursts were forced by ice precipitation loading and melting and unsaturated air entrainment into the mixed-phase precipitation core. In addition, a trailing stratiform precipitation region with possible embedded elevated convective storm cells enhanced the severity and longevity of the QLCS during its track through the greater London area and southeastern England. The favorable thermodynamic and dynamic factors revealed in this study warrant further investigation into the potential role of elevated convection and the development of a rear-inflow jet during the most intense phase of the system. Comparison of LEO satellite microwave imagery to Doppler radar reflectivity patterns and cross-sections of WRF-model derived thermodynamic parameters (i.e., equivalent potential temperature) should further strengthen the evidence for QLCS structure and the presence of a rear-inflow jet.

## NUCAPS Sounding: Loughborough, Leicestershire, UK



**Microburst Potential Index** Init: 2022-10-23 06:00:00  
Value: 2022102312      **Microburst Potential Index** Init: 2022-10-23 06:00:00  
Value: 2022102314      **Microburst Potential Index** Init: 2022-10-23 06:00:00  
Value: 2022102316

**1222 UTC NUCAPS MWPI Max Gust = 21.1 ms<sup>-1</sup>**

Courtesy of David Smart, TORRO/UCL Hazard Centre

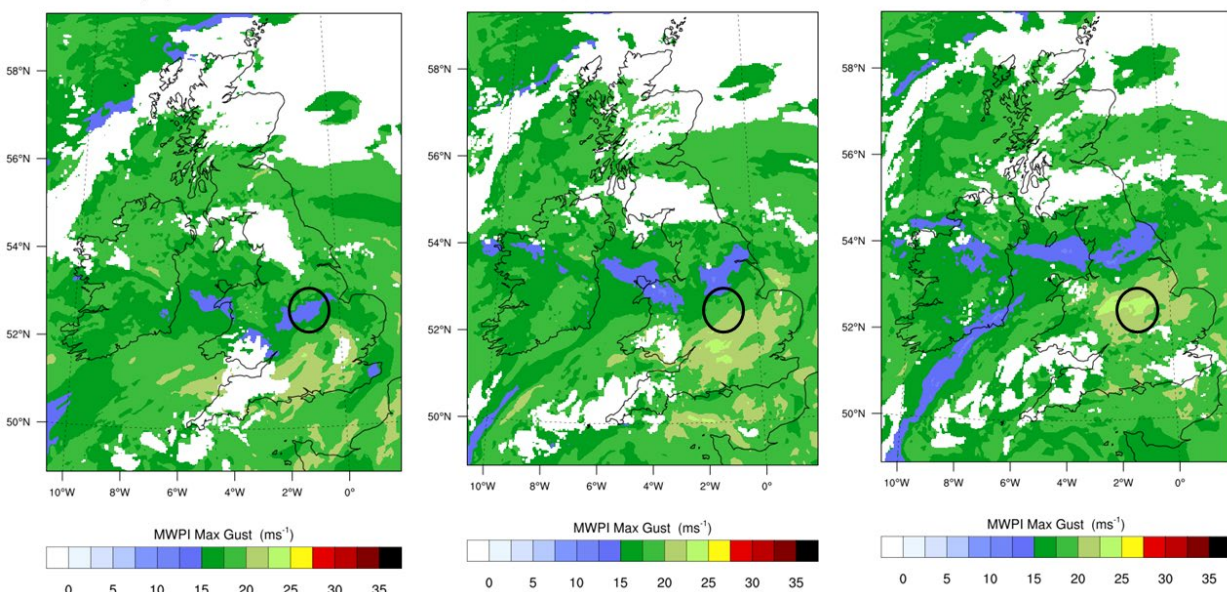
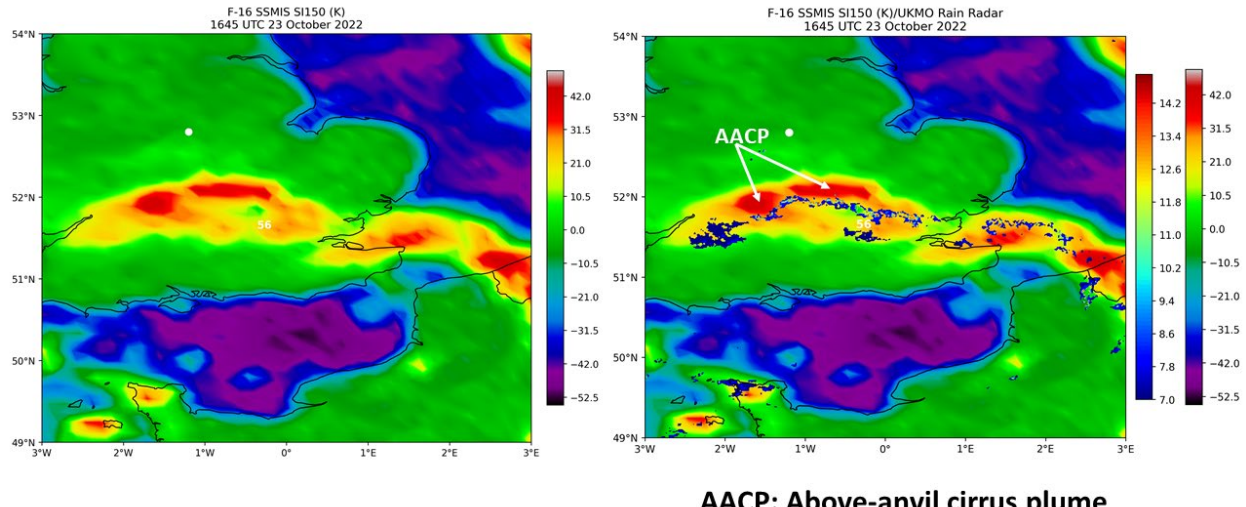


Figure 1. Comparison of the NUCAPS sounding profile over Leicestershire, UK to the WRF sounding profile over London Heathrow Airport during the afternoon of 23 October 2022 (top); WRF model-derived MWPI product over the UK between 1200 and 1600 UTC 23 October 2022 (bottom).

## SSMIS-Radar Product Comparison



## SSMIS-Radar Product Comparison

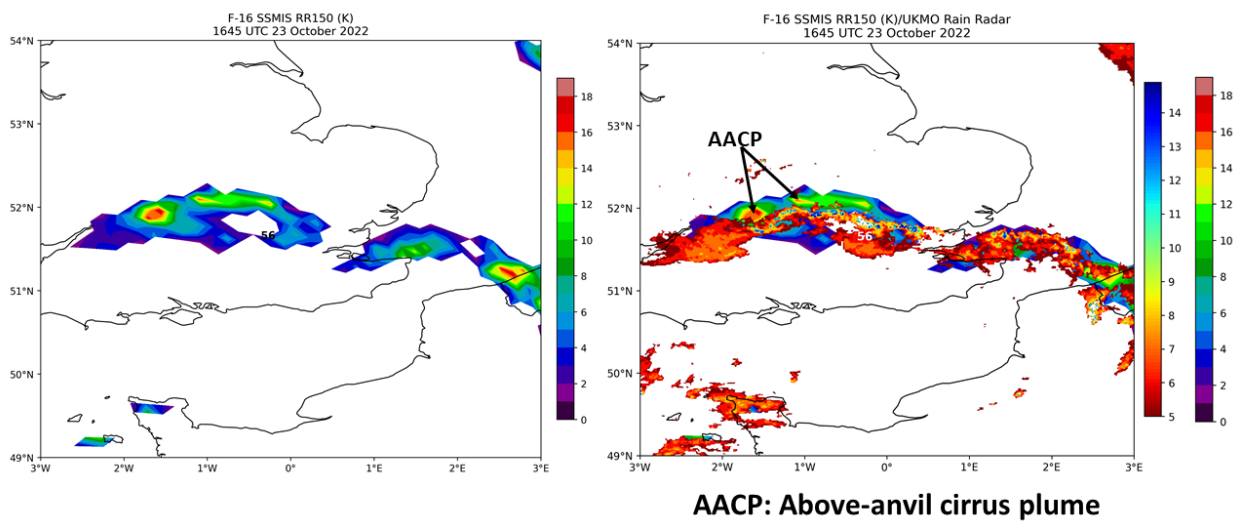


Figure 2. Comparison of DMSP SSMIS-derived scattering index (“SI”) and calculated rain rate (mm/hr, top) to UKMO radar-derived rain rate (mm/hr, bottom) at 1645 UTC 23 October 2022.

### 1. Introduction

Cool-season convective storms over northwestern Europe and Great Britain continue to be a forecasting challenge as well as a public safety hazard, especially during periods of unseasonably warm temperatures and associated enhanced instability. During the afternoon of 23 October 2022,

a quasi-linear convective system (QLCS), with a morphological evolution more typical of the warm season over continental Europe (Gatzen 2004; Mathias et al. 2017), developed and intensified over the English Channel and tracked north-northeastward into southern England. The atypically large potential instability established over central and southern England and structural characteristics of the convective elements of the system promoted widespread damaging downburst winds. The highest measured downburst wind gusts of the event occurred at 1) Army Aviation Centre (AAC) Middle Wallop, Hampshire (55 miles SW of London), with a wind gust of 54 kt (62 mph) recorded between 1500 and 1600 UTC and generated by a prominent bowing segment of the QLCS; 2) London Colney, Hertfordshire, with a wind gust of 56 kt (64 mph) recorded at 1640 UTC and generated by a pulse-severe cell east of the bowing segment of the QLCS. The favorable thermodynamic and dynamic factors revealed in this study warrant further investigation into the potential role of elevated convection and the development of a rear-inflow jet during the most intense phase of the system (Weisman 1992; White et al. 2016). Comparison of LEO satellite microwave imagery to Doppler radar reflectivity patterns and cross-sections of WRF-model derived thermodynamic parameters (i.e., equivalent potential temperature) should further strengthen the evidence for QLCS structure and the presence of a rear-inflow jet. Figure 1, a WRF-model simulation of the QLCS during phase 1, summarizes the favorable thermodynamic and dynamic factors that promoted strong outflow wind generation (Pryor 2022a; Pryor 2022b): 1) precipitation loading, 2) latent cooling, 3) negative buoyancy ( $F_{down}$ ), 4) downdraft acceleration, 5) downshear wake entrainment, and 6) rear-flank circulation/rear-inflow jet. This research effort demonstrates how ground-based and satellite-based observational data for convective storms can be combined for monitoring and forecasting applications. In addition, this paper will highlight the scientific value added by synergistic analysis of satellite and ground-based sensor datasets.

## 2. Data and Methodology

The NOAA-Unique Combined Atmospheric Processing System (NUCAPS, Nalli et al. 2020, Kalluri et al. 2022) is an enterprise algorithm that retrieves atmospheric profile environmental data records (EDRs), and is applied and evaluated for both a daytime and nocturnal severe convective windstorm cases. NUCAPS is also the primary algorithm for the operational hyperspectral thermal IR and microwave sounders (i.e. Advanced Technology Microwave Sounder (ATMS), Cross-track Infrared Sounder (CrIS)). The ATMS and CrIS instruments are deployed on the NOAA-operational low earth orbit (LEO) Joint Polar Satellite System (JPSS)-series satellites. For this study, NUCAPS sounding profiles, retrieved over West Sussex and Leicestershire, respectively, at midday (1222 UTC) were compared with co-located 1200 UTC radiosonde observation (RAOB) soundings. The NUCAPS soundings provided a lead time of three hours before the onset of the QLCS over southern England. Figure 2 graphically summarizes the structure of the NUCAPS enterprise algorithm.

Figure 3 illustrates the rigorous inter-comparison process employed to infer and extract the most important physical processes that sustained the QLCS and fostered intense outflow winds. The most important steps in the evaluation process entail pattern recognition, parameter evaluation, and feature identification applying coincident sounding retrieval and satellite, radar and NWP model 2-D plan-view images to build a three-dimensional conceptual model. Due to the optimal timing of satellite overpasses and attendant retrievals with respect to the most intense phase of the QLCS, the Defense Meteorological Satellite Program (DMSP) F-16 and F-18 satellite Special Sensor Microwave Imager Sounder (SSMIS) datasets were employed to extract the most

important patterns related to severe convection and downburst occurrence. The SSMIS is a conical scanner with a  $53.1^\circ$  zenith angle, swath width 1700 km, scan rate of 31.9 scans/min, which equals 12.5 km/scan. SSMIS 91GHz window channel and the 150 GHz and 183 ( $\pm 7$ ) GHz water vapor sounding channel datasets were obtained from the NOAA Comprehensive Large Array-data Stewardship System (CLASS) and employed for the purpose of storm microphysical analysis. For the SSMIS, dual-polarized 91 GHz brightness temperature datasets allow for the calculating polarization-corrected temperature (“PCT”, Liu et al. 1995), while the difference between the horizontally-polarized 91 GHz and 150 GHz brightness temperature defines the scattering index (SI, Ferraro et al. 2000). In addition, Integrated Multi-satellitE Retrievals for GPM (IMERG) precipitation rate product imagery was obtained from the National Aeronautics and Space Administration (NASA) Goddard Earth Sciences Data and Information Services Center for the event time of interest. IMERG combines information from the Global Precipitation Measurement (GPM) satellite constellation to estimate precipitation over the majority of the Earth's surface, and for this study, was visualized to evaluate the overall morphology and intensity of the QLCS. To compare directly with passive microwave sounding imagery, the UK currently has a network of 16 C-band, dual polarisation, Doppler radars. Short pulse data, with a maximum range of 115 km, are analysed from two radars in the storm impact area (Dean Hill and Chenies). The single site scans from these radars, with beam width 1 degree and range gates every 0.6 km, were capable of generating imagery with the resolution required to identify embedded mesoscale features of the QLCS, including bow echoes, supercells, line-end and leading-line vortices.

The Met Office Unified Model—JULES Regional Atmosphere and Land configuration version 2 for the midlatitudes (RAL2M; Bush et al. 2023) was used to create a downscaled 2.2 km grid length with 90 vertical levels simulation of the event initiated at 0300 UTC 23 October 2022. Key features of the UCL WRF-model run configuration are described in Figure 4. The planetary boundary layer, shallow convection and microphysics schemes were selected to provide the best depiction of the radar-observed convective features in this case. Relatively little work has been published on the performance of WRF in convective environments in the UK and work is on-going to refine the selection of parametrisations<sup>1</sup>.

### **3. Phase I: Dorset-Hampshire-Sussex, UK Bow Echo and Supercell**

The first phase of the QLCS lifetime over southern England, denoted in Figure 5, entailed its track from the English Channel northward into Dorset and Hampshire between 1430 and 1500 UTC. As shown in Figures 6 and 7, the QLCS developed a prominent bowing segment on its western (left) flank over the English Channel that persisted during its track through south-central England. The squall line bow echo (Klimowski et al. 2004) merged with a supercell storm over Bournemouth near 1445 UTC and then proceeded north-northeastward into Hampshire, producing a series of tornadoes and severe downbursts. Shortly after 1600 UTC, the SSMIS PCT and 183 ( $\pm 7$ ) GHz brightness temperature product images displayed the general bowing structure of the QLCS and a prominent rear-inflow notch over Hampshire in Figure 6. Near this time, the bow-echo complex was moving through Wiltshire and Berkshire, succeeding the 54-kt ( $28 \text{ ms}^{-1}$ ) magnitude downburst wind event at Middle Wallop and the EF-1 intensity long-track tornado through Hampshire. Corresponding Doppler radar imagery more clearly displayed the western bookend vortex and an area of localized rotation associated with the bow echo-supercell merger

---

<sup>1</sup> The reader is referred to [https://www2.mmm.ucar.edu/wrf/users/physics/phys\\_references.html](https://www2.mmm.ucar.edu/wrf/users/physics/phys_references.html) for further details on WRF physics options.

over northern Hampshire. Storm-scale interaction and morphological evolution was effectively depicted in the IMERG precipitation rate imagery in Figure 7 as the QLCS was tracking through Dorset, Hampshire, and West Sussex between 1500 and 1600 UTC. The remarkably low PCTs and 183 GHz channel BTs below 180 K signified the enhancement of mixed and ice-phase precipitation loading within the bow-echo complex (Klimowski et al. 2004) thereby further strengthening the system cold pool.

Doppler radar and IMERG imagery most clearly showed the QLCS-supercell merger over Hampshire and the resulting bow echo enhancement following the process described by French and Parker (2012, "FP12"). The merger over Hampshire closely resembled the "system-scale bowing evolution" based on radar reflectivity analysis as designated by FP12, and, in this case, was associated with the generation of severe downburst winds promoted by cold pool enhancement. The precipitation rate gradient also shown in Figure 7 indicated locally higher gradient values immediately downstream of the bow echo apex during its track through northern Hampshire, suggesting that downshear wake entrainment of unsaturated air likely had a role in downburst generation. Figure 8, a qualitative comparison of NUCAPS and WRF model soundings over Hampshire and Sussex, revealed favorable conditions for intense storm downdraft generation and resultant strong outflow winds with close agreement between the boundary layer structure ("inverted-V") as resolved by the NUCAPS soundings and WRF profiles and the microburst windspeed potential index (MWPI, Pryor 2015) gust potential as calculated from NUCAPS and the WRF model. Various NWP model diagnostic products displayed in Figures 9 and 10, including the CAPE ratio and MWPI maximum wind gust potential, respectively, indicated a high likelihood of surface-based convective storm development that would produce damaging downburst winds, especially near the bow echo apex. 1200 UTC NUCAPS and WRF model MWPI-calculated wind gust potential of 40 to 44 kt (20 to 22.5 ms<sup>-1</sup>), with the addition of a surface to 3 km mean wind of 19 kt, yielded a total wind gust potential 59 to 63 kt (30 to 32 ms<sup>-1</sup>) which was only slightly greater than the observed wind gust magnitude at Middle Wallop.

#### 4. Phase II: London and Southeastern England Bow Echo

The second phase of the QLCS lifetime entailed its track from Wiltshire-Berkshire-Kent, merger with a supercell over Greater London, and then northward into the Midlands between 1600 and 1800 UTC. This phase also represents the second instance of a noteworthy QLCS-supercell merger of the severe storm event. As shown in Figures 11 – 13, the QLCS developed a prominent bowing segment west of London that persisted during the remainder of its track. Unlike the merger during phase I, the QLCS-supercell merger over London resulted in a cluster of pulse-severe storms that produced a succession of downbursts over Hertfordshire between 1640 and 1740 UTC. During this period, a prominent stratiform precipitation region, with embedded elevated convective storm activity, propagated in the wake of the pulse storm cluster. F-16 SSMIS 150 GHz retrievals were available for the pass over southeastern England, as shown in Figure 11, allowing for the calculation of the scattering index and the inference of the presence of anvil cirrus plumes immediately downshear of the leading convective storm line of the QLCS. The general system-scale bowing of the squall line is still apparent in IMERG imagery in Figure 12 with a relative increase in the precipitation rate gradient on the upshear flank of the trailing elevated convection region, suggesting an increase in rear inflow. Doppler radar velocity imagery in Figure 13 confirms the increase in rear inflow toward the region of the QLCS-supercell merger where a localized embedded bow echo developed over southern Hertfordshire. Shortly after the merger, one of the

strongest downburst wind gusts of the event, 56 kt ( $29 \text{ ms}^{-1}$ ), was recorded by a WeatherFile sonic wind sensor at Phoenix Model Club ("PMC" in Figure 13).

In a similar manner to the sounding analysis for phase I, Figure 14 signified the favorable conditions for intense storm downdraft generation and resultant strong outflow winds with close agreement between the boundary layer structure ("inverted-V") as resolved by the NUCAPS and RAOB soundings and WRF profiles. The NWP model convection diagnostic products visualized in Figures 15 and 16, including the CAPE ratio and maximum column integrated graupel, echo the patterns and magnitudes displayed in the satellite and radar imagery in Figures 11 – 13. This associative relationship suggests that expanding areal extent of the trailing stratiform region with elevated convective storm development and increasing ice-phase precipitation content resulted in an enhancement in cold pool strength and rear-inflow jet (RIJ) intensification during the track of the QLCS through the greater London region.

## 5. Discussion and Conclusions

The strategic application of polar-orbiting meteorological satellite and ground-based microwave (radar) datasets allowed for the comprehensive tracking of the QLCS through most of its life-cycle. In addition to application of high-resolution, convection-allowing numerical prediction models, coordinated monitoring of the thermodynamic structure and associated stability of the lower troposphere with co-located satellite and ground-based sounding retrievals provided an effective operational demonstration.

In general, the early afternoon (1222 UTC) NOAA-20 NUCAPS sounding qualitatively indicated the strongest signal for severe thunderstorm and downburst occurrence over southern England: Close agreement between the boundary layer structure ("inverted-V") as resolved by the NUCAPS soundings and WRF profiles and the MWPI gust potential as calculated from NUCAPS and the WRF model. A strong relationship is noted between high rain rates as indicated by UKMO radar, IMERG product imagery, and the very low MW brightness temperatures (BTs) apparent in both the consecutive F-18 and F-16 overpasses. Low BTs also correspond well with the high integrated graupel values, suggesting that intense downdrafts and resulting downbursts were forced by ice-phase precipitation loading and melting, as well as unsaturated air entrainment into the mixed-phase precipitation core.

Diagnostics to determine the environment that the convection formed in, from Flack et al. (2023), show that the event was initially surface-based. However, as time progressed and the convective cores stabilized the environment, the rear of parts of the QLCS had elements of elevated instability influencing the convection. This elevated instability may help explain the increased precipitation rates within the stratiform region of the QLCS and investigations are still ongoing. Future work will consist of further exploration of the role of squall line-supercell mergers in the enhancement and promotion of severe straight-line winds and tornadogenesis in close proximity. This phase of the study will likely entail higher resolution model simulations that are more sensitive to precipitation phase and concentration and boundary layer turbulence.

## References

- Bush, M., Boutle, I., Edwards, J., Finnenkoetter, A., Franklin, C., Hanley, K., Jayakumar, A., Lewis, H., Lock, A., Mittermaier, M., Mohandas, S., North, R., Porson, A., Roux, B., Webster, S., and Weeks, M. 2023: The second Met Office Unified Model–JULES Regional Atmosphere and

Land configuration, RAL2, Geosci. Model Dev., 16, 1713–1734, <https://doi.org/10.5194/gmd-16-1713-2023>.

Ferraro, R. R., F. Weng, N. C. Grody, and L. Zhao, 2000: Precipitation characteristics over land from the NOAA-15 AMSU sensor. Geophysical Research Letters, 27(17), pp.2669-2672.

Flack, D.L.A., Lehnert, M., Lean, H.W., and Willington S. (2023) Characteristics of Diagnostics for Identifying Elevated Convection over the British Isles in a Convection-Allowing Model. Wea. Forecasting 38: 1079-1094, <https://doi.org/10.1175/WAF-D-22-0219.1>

French, A. J., and M. D. Parker, 2012: Observations of Mergers between Squall Lines and Isolated Supercell Thunderstorms. Wea. Forecasting, 27, 255–278, <https://doi.org/10.1175/WAF-D-11-00058.1>

Gatzen, C., 2004: A Derecho in Europe: Berlin, 10 July 2002. Wea. Forecasting, 19, 639–645, DOI: [https://doi.org/10.1175/1520-0434\(2004\)019<0639:ADIEBJ>2.0.CO;2](https://doi.org/10.1175/1520-0434(2004)019<0639:ADIEBJ>2.0.CO;2)

Kalluri, S., C. Barnet, M. Divakarla, R. Esmaili, N. Nalli, K. Pryor, T. Reale, N. Smith, C. Tan, T. Wang, J. Warner, M. Wilson, L. Zhou, and T. Zhu, 2022: Validation and Utility of Satellite Retrievals of Atmospheric Profiles in Detecting and Monitoring Significant Weather Events. Bulletin of the American Meteorological Society, 103, E570-E590, <https://doi.org/10.1175/BAMS-D-20-0126.1>

Klimowski, B. A., M. R. Hjelmfelt, and M. J. Bunkers, 2004: Radar Observations of the Early Evolution of Bow Echoes. Wea. Forecasting, 19, 727–734, [https://doi.org/10.1175/1520-0434\(2004\)019<0727:ROOTEE>2.0.CO;2](https://doi.org/10.1175/1520-0434(2004)019<0727:ROOTEE>2.0.CO;2).

Liu, G., J.A. Curry, and R.W. Sheu, 1995: Classification of clouds over the western equatorial Pacific Ocean using combined infrared and microwave satellite data. Journal of Geophysical Research: Atmospheres, 100(D7), 13811-13826.

Mathias, L., V. Ermert, F. D. Kelemen, P. Ludwig, and J. G. Pinto, 2017: Synoptic Analysis and Hindcast of an Intense Bow Echo in Western Europe: The 9 June 2014 Storm. Wea. Forecasting, 32, 1121–1141. DOI: 10.1175/WAF-D-16-0192.1

Nalli, N.R., C. Tan, J. Warner, M. Divakarla, A. Gambacorta, A.; M. Wilson, T. Zhu, T. Wang, Z. Wei, K. Pryor, S. Kalluri, L Zhou, C. Sweeney, B. C. Baier, K. McKain, D. Wunch, N. M. Deutscher, F. Hase, L. T. Iraci, R. Kivi, I. Morino, J. Notholt, H. Ohyama, D. F. Pollard, Y. Té, V. A. Velazco, T. Warneke, R. Sussmann, M. Rettinger, 2020: Validation of Carbon Trace Gas Profile Retrievals from the NOAA- Unique Combined Atmospheric Processing System for the Cross-Track Infrared Sounder. Remote Sens., 12, 3245. <https://doi.org/10.3390/rs12193245>

Pryor, K. L., 2015: Progress and developments of downburst prediction applications of GOES. Wea. Forecasting, 30, 1182–1200, <https://doi.org/10.1175/WAF-D-14-00106.1>

Pryor, K. L., and B. Demoz, 2022: A Retrospective Satellite Analysis of the June 2012 North American Derecho. Remote Sensing, 14(14), 3479; <https://doi.org/10.3390/rs14143479>

Pryor, K. L., 2022a: Examination of the Physical Process of Severe Convective Windstorms [Doctoral dissertation]. University of Maryland, Baltimore County.

Pryor, K.L., 2022b: “Downburst monitoring and prediction studies”. Field Measurements for Passive Environmental Remote Sensing, Elsevier, Cambridge, MA, 2022, pp. 411–429.

Weisman, M. L., 1992: The role of convectively generated rear inflow jets in the evolution of long-lived mesoconvective systems. J. Atmos. Sci., 49, 1826–1847.

White, B. A., A. M. Blyth, and J. H. Marsham, 2016: Simulations of an observed elevated mesoscale convective system over southern England during CSIP IOP 3. Q.J.R. Meteorol. Soc., 142, 1929–1947. <https://doi.org/10.1002/qj.2787>

## Figures

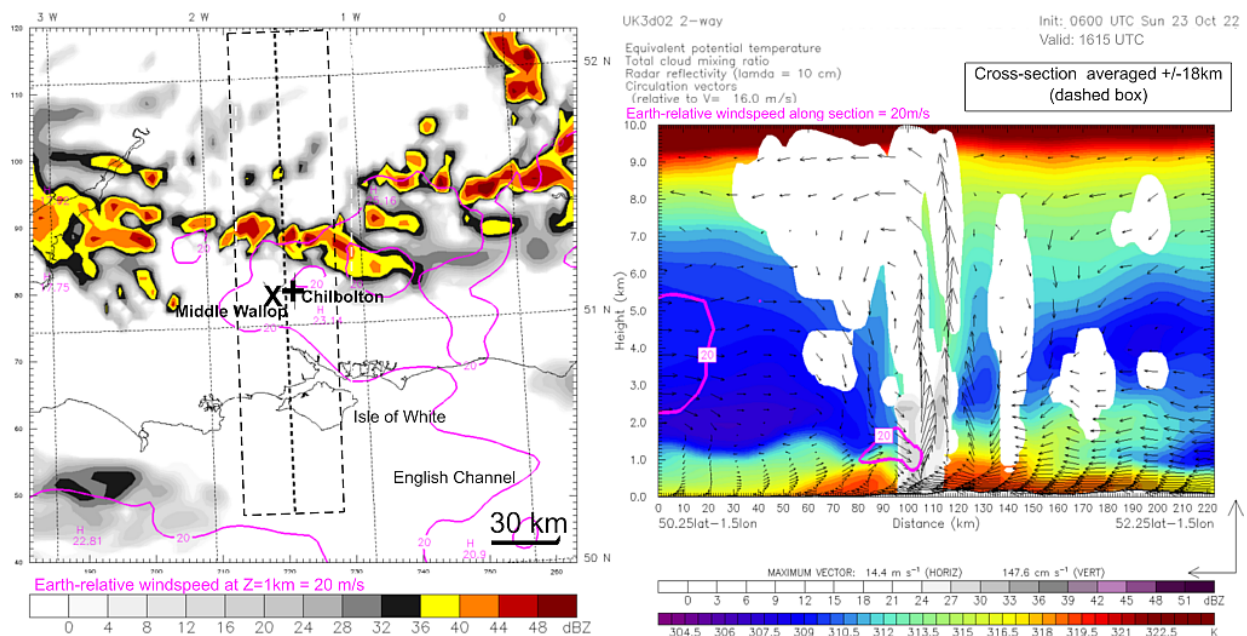


Figure 1. A deep convective storm with the potential to generate intense downdrafts and damaging downburst winds: plan view of WRF model-simulated radar reflectivity over southern England (left) and cross-section (right) at 1615 UTC 23 October 2022. Figure generated from a one-way nested 9-3km/38 level convection-permitting WRF run initialised with Global Forecast System data. The cross-section is averaged over a 36km-wide box.

## NUCAPS Enterprise Algorithm

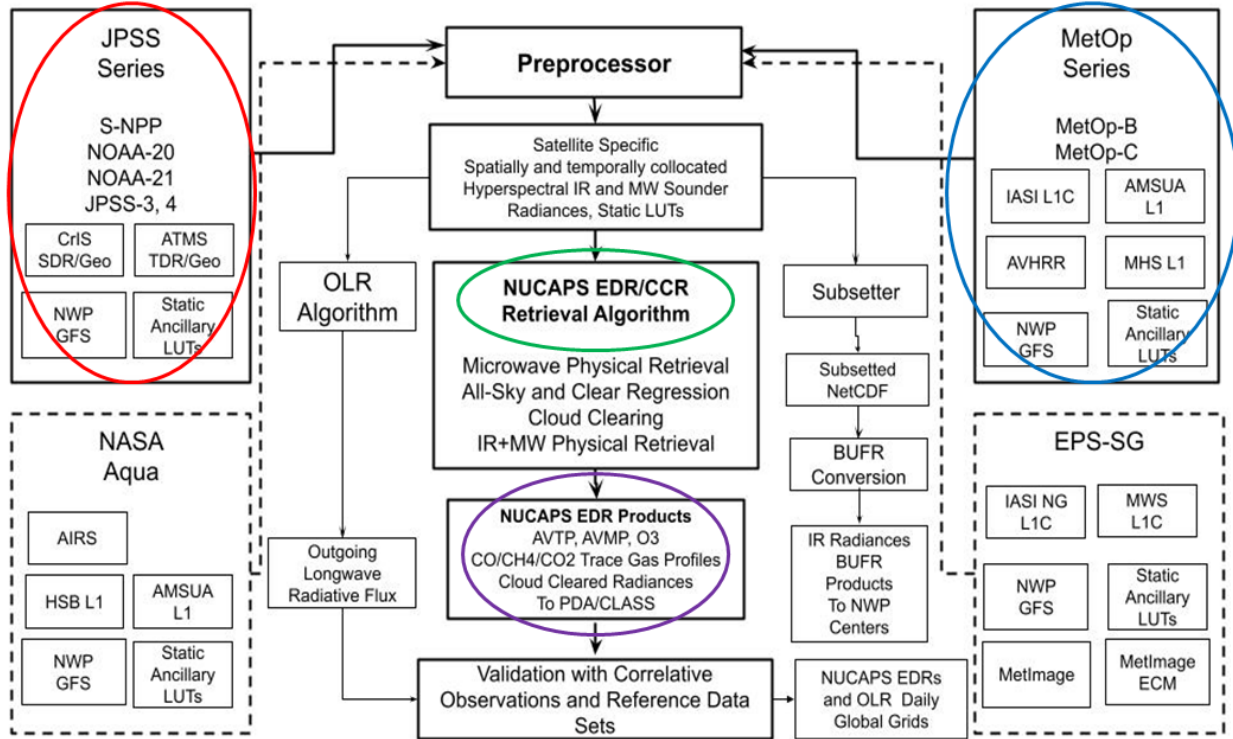


Figure 2. Graphical summary of the NUCAPS enterprise algorithm.

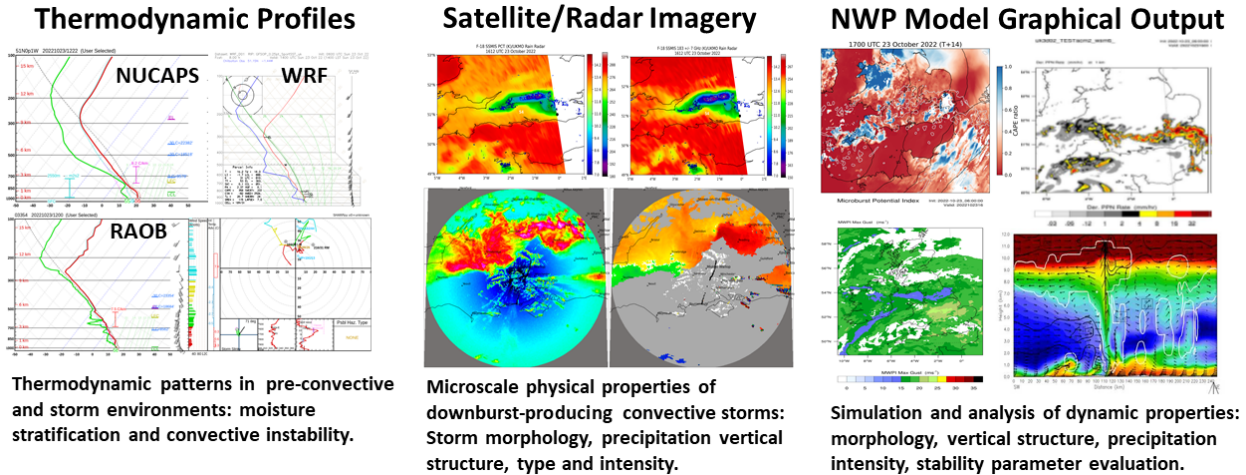


Figure 3. Graphical summary of data analysis and methodology for this study.

# 'Operational' WRF

- WRF-ARW 4.2.x (modified code)
- Init GFS 06Z 0.25 deg ptiles
- 9-3km/38L (lowest ~40m)
- Deep Cu OFF, GRIMs shallow Cu ON.
- WSM6 single moment physics (inc graupel)
- ACM2 local/non-local PBL
- Noah LSM
- 1-way nesting (concurrent, every time step)

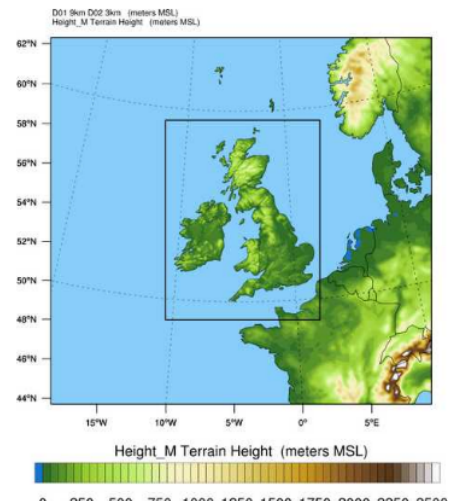


Figure 4. Specifications for the WRF model configuration employed for this study (courtesy of D. Smart, UCL Hazard Centre, Univ. College London).

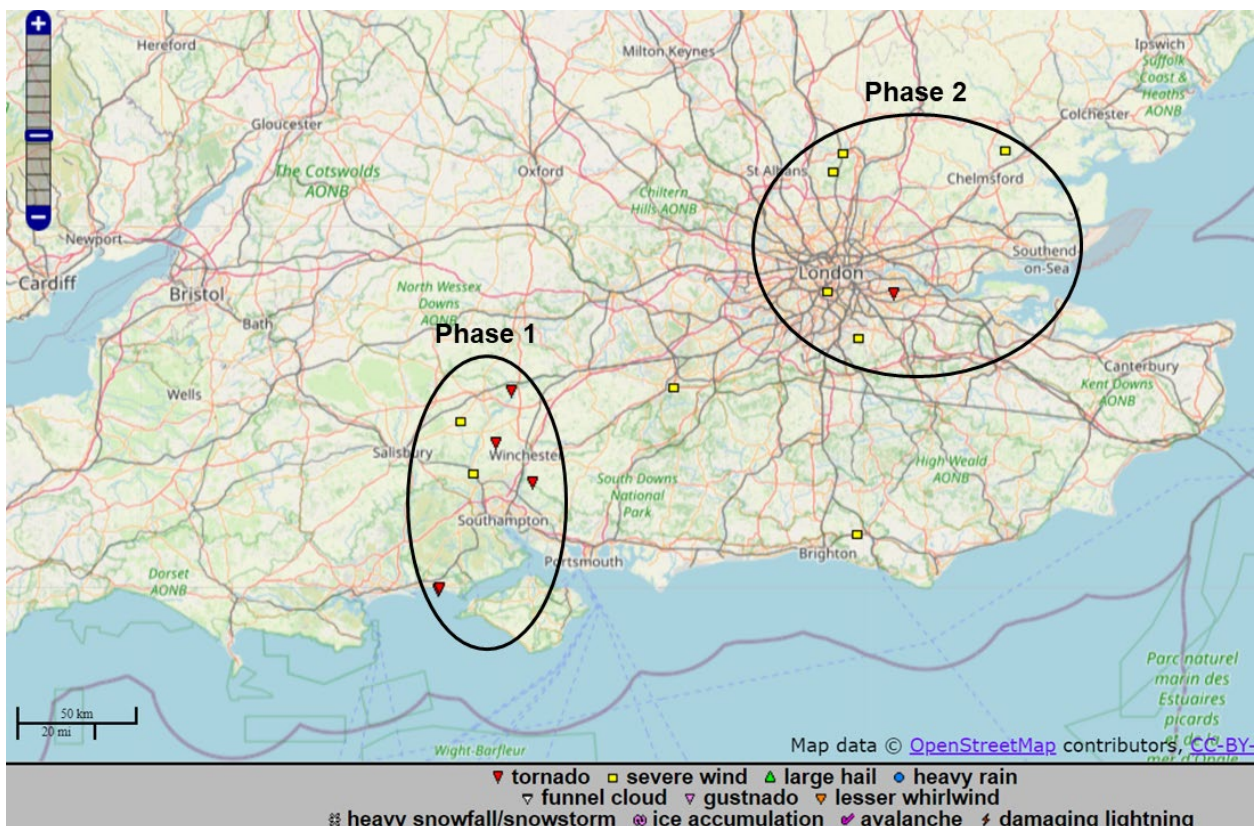


Figure 5. European Severe Weather Database (ESWD) storm reports over Great Britain on 23 October 2022.

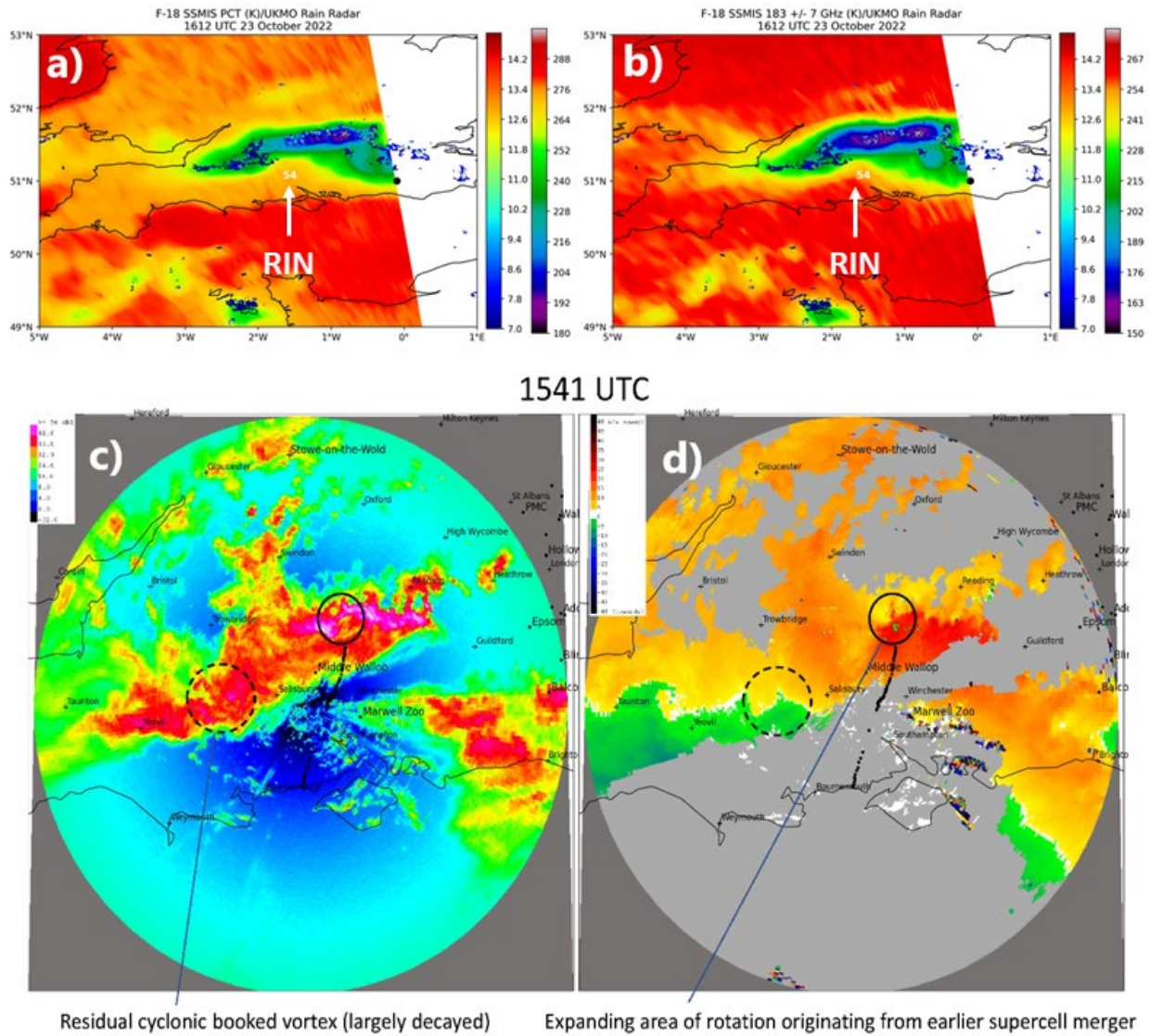


Figure 6. F-18 SSMIS a) polarization-corrected temperature (PCT, K) and b) 183 +/- 7 GHz brightness temperature with overlying UKMO radar rain rate at 1612 UTC and Dean Hill, UK c) radar reflectivity and d) radar velocity at 1541 UTC 23 October 2022. “RIN” denotes a rear-inflow notch.

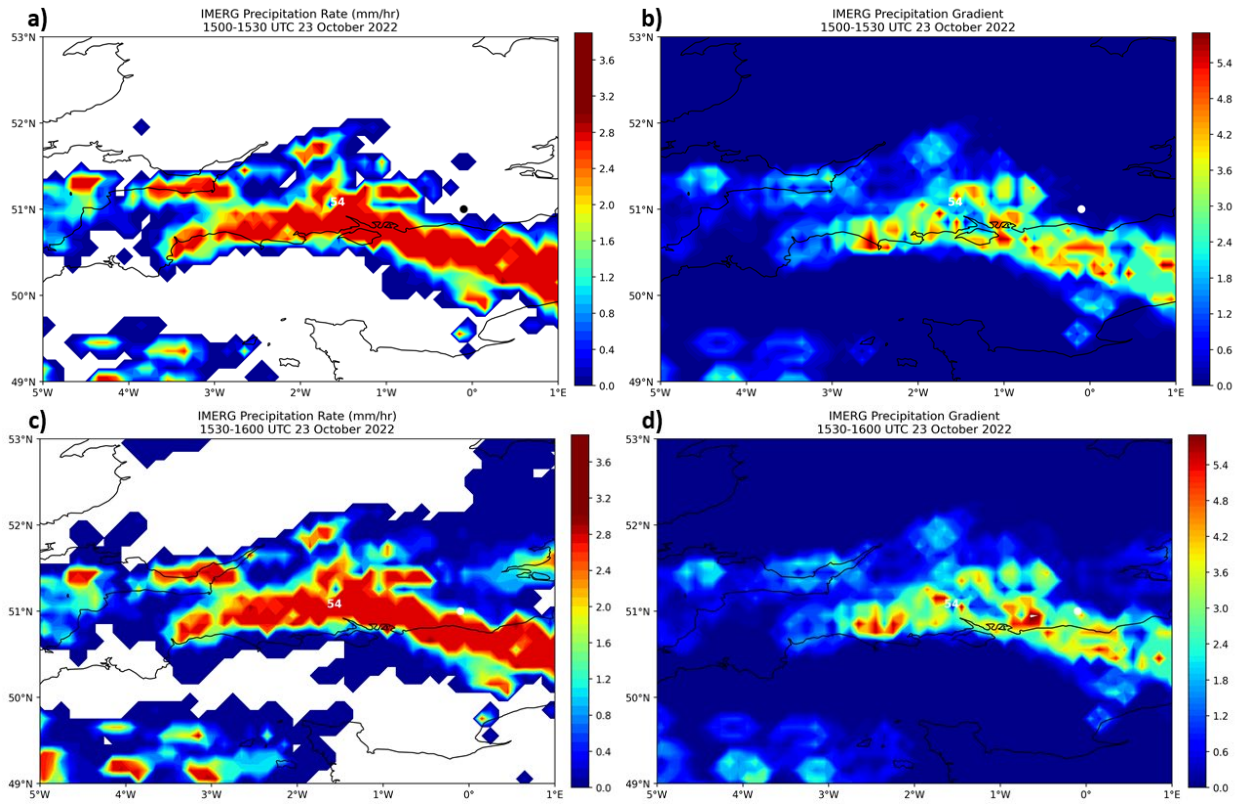


Figure 7. Integrated Multi-satellite Retrievals for GPM (IMERG) precipitation rate (mm/hr) on 23 October 2022 at a) 1500-1530 UTC and c) 1530–1600 UTC; and IMERG precipitation rate gradient at b) 1500-1530 UTC and d) 1530-1600 UTC.

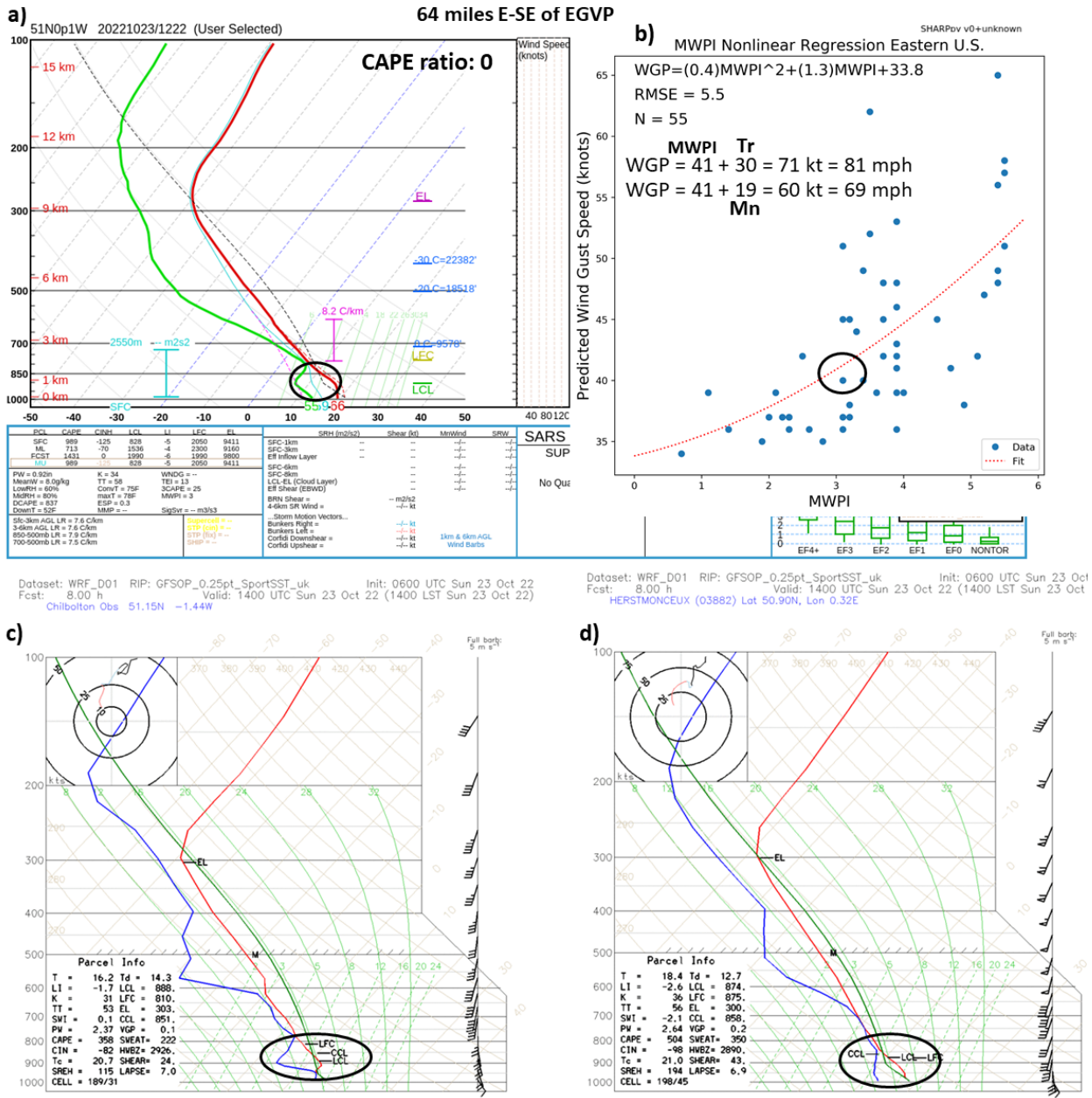


Figure 8. NUCAPS and WRF model sounding comparison: a) NUCAPS sounding profile over Haywards Heath, West Sussex at 1222 UTC with the b) MWPI regression chart demonstrating the wind gust potential calculation technique, and WRF-model generated sounding profiles over c) Chilbolton Observatory, near Stockbridge, Hampshire and d) Herstmonceux, East Sussex at 1400 UTC 23 October 2022.

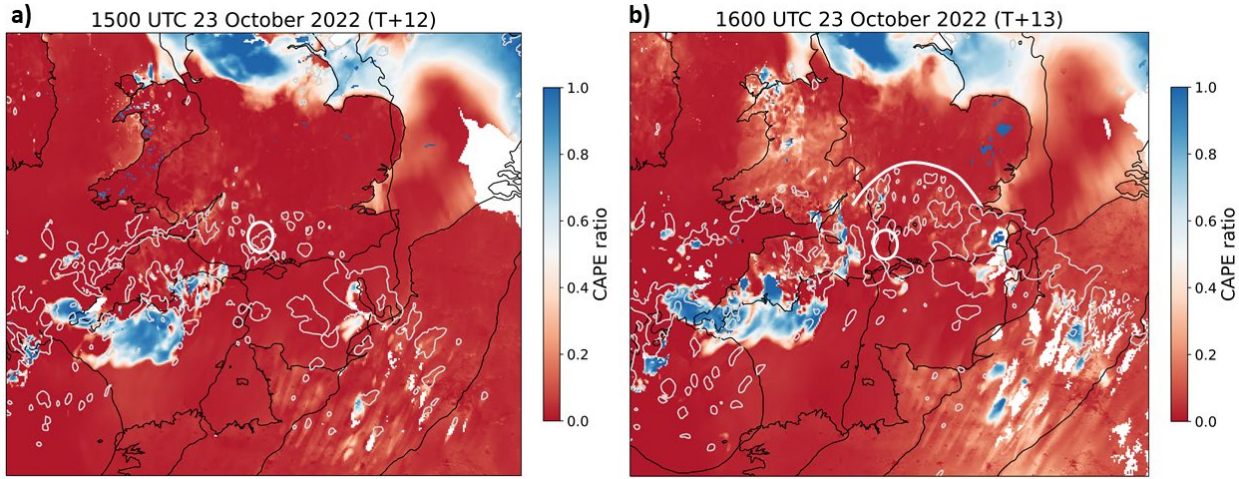


Figure 9. CAPE ratio diagnostic ( $1 - (\text{SBCAPE}/\text{MUCAPE})$ ) map from the UM forecasts of the 23 October 2022 QLCS: a) 1500 UTC and b) 1600 UTC. Reds indicate environments suitable for surface-based convection, blues indicate environments suitable for elevated convection. The gray contours show the 30 dBZ model reflectivity, and the black contours the MSLP. The white circle marks the location of downburst occurrence at Middle Wallop while the white arc represents the leading edge of the bowing segment of the QLCS over the Midlands.

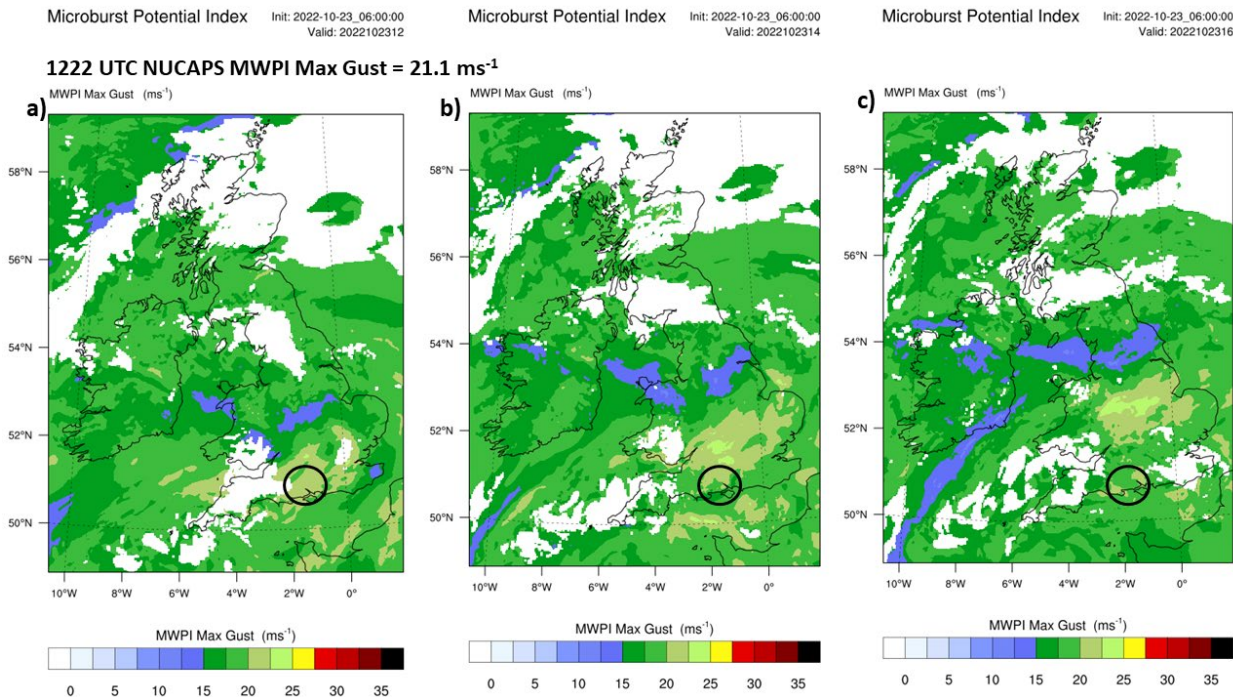


Figure 10. UK sector WRF model-derived MWPI maximum wind gust potential maps at a) 1200 UTC, b) 1400 UTC, and c) 1600 UTC 23 October 2022 (courtesy of D. Smart, UCL Hazard Centre, Univ. College London).

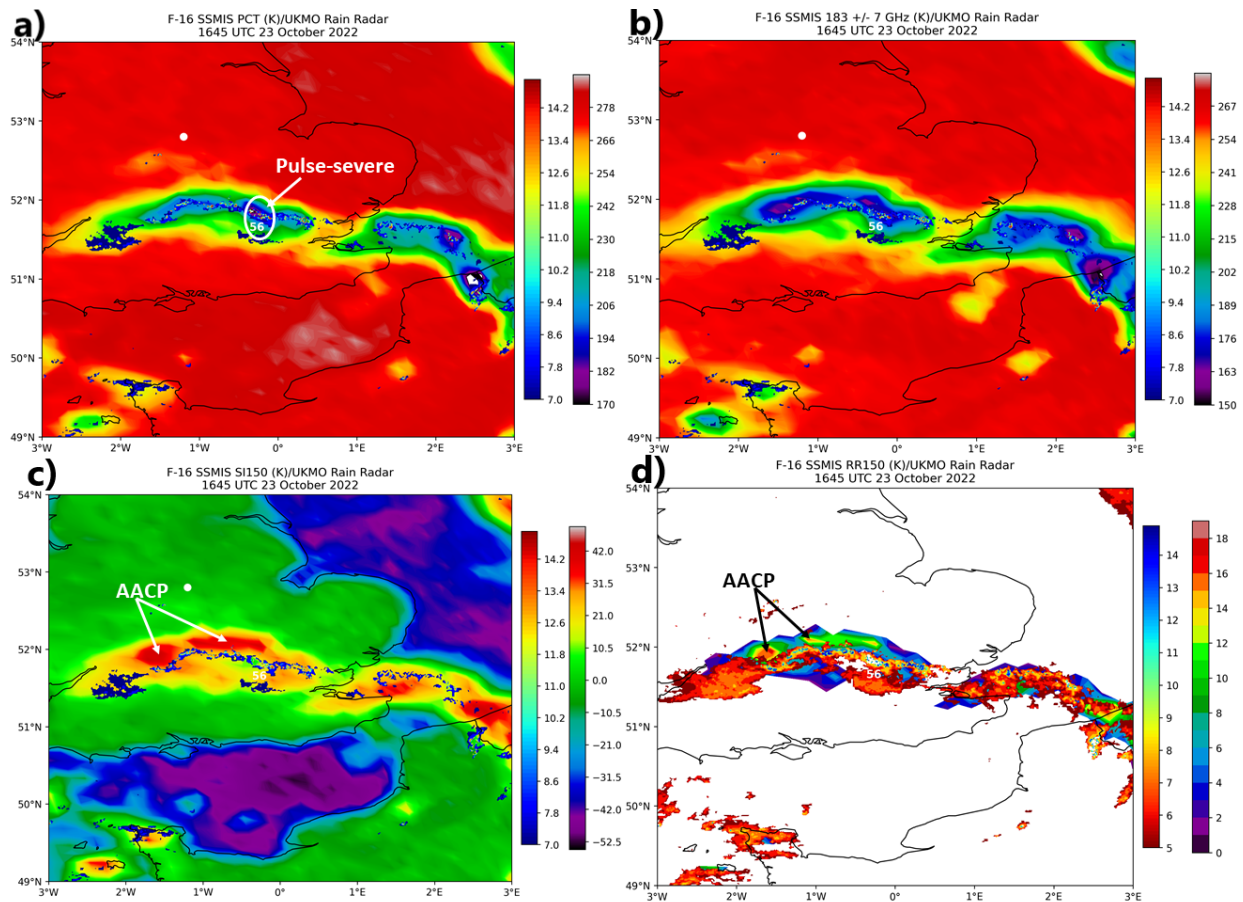


Figure 11. F-16 SSMIS a) polarization-corrected temperature (PCT, K), b) 183 +/- 7 GHz brightness temperature (K), c) 150 GHz scattering index (SI), and d) 150 GHz-channel derived rainfall rate (RR150) with overlying UKMO radar rainfall rate at 1645 UTC 23 October 2023.

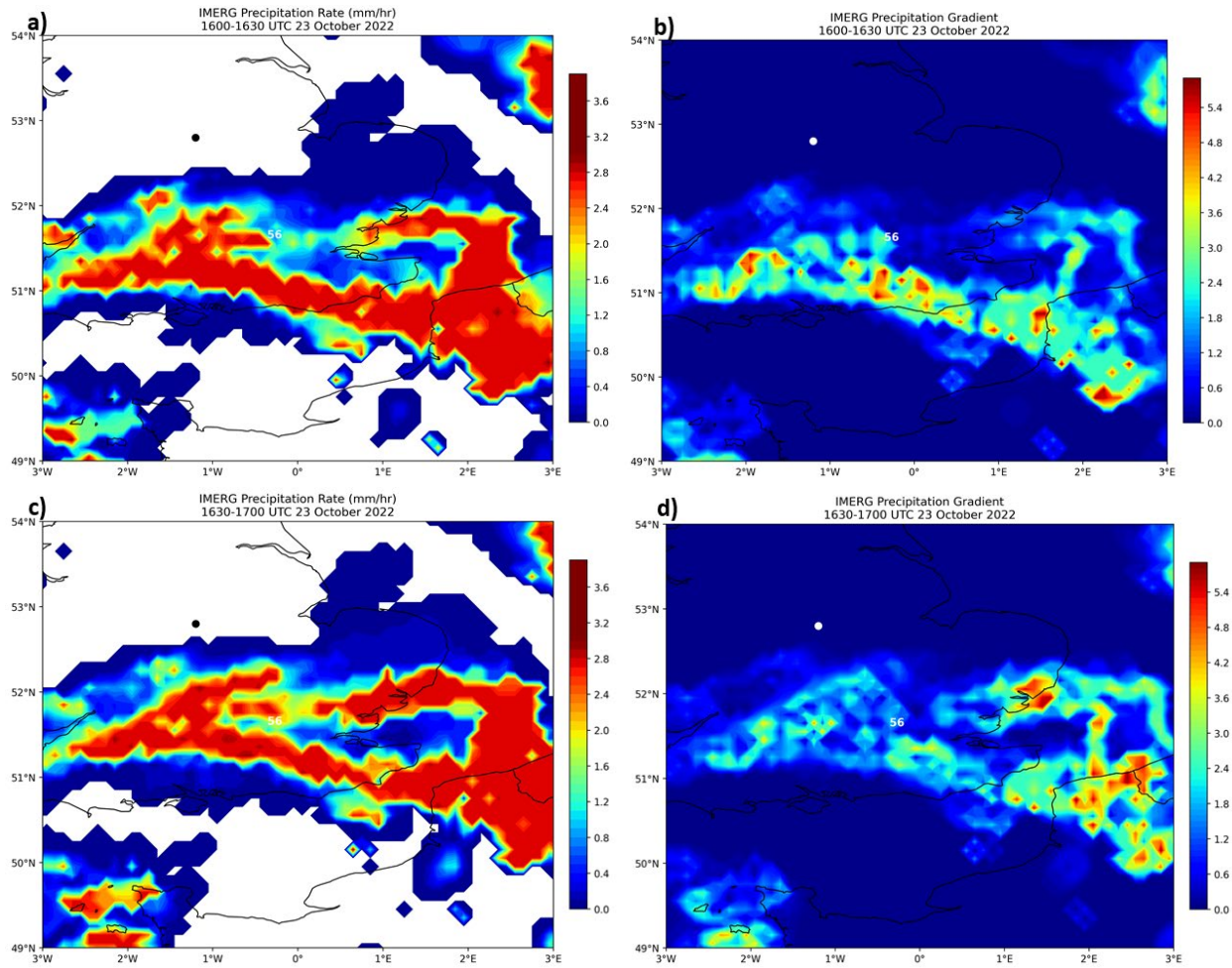
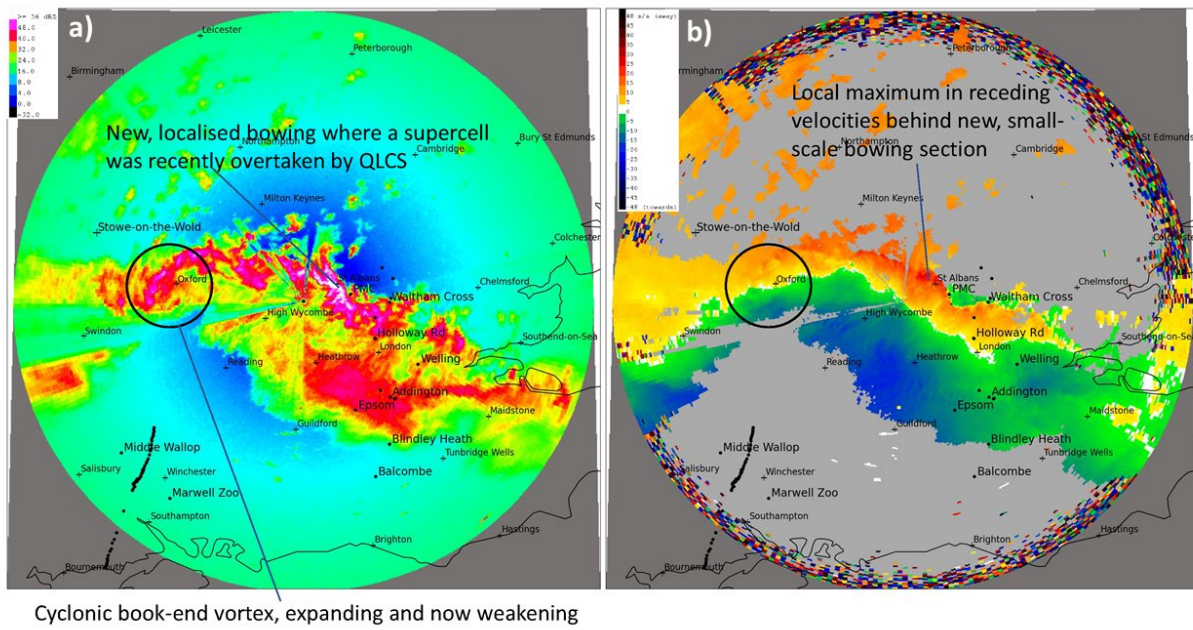


Figure 12. Integrated Multi-satellite Retrievals for GPM (IMERG) precipitation rate (mm/hr) on 23 October 2022 at a) 1600-1630 UTC and c) 1630–1700 UTC; and IMERG precipitation rate gradient at b) 1600-1630 UTC and d) 1630-1700 UTC.

1631 UTC



Cyclonic book-end vortex, expanding and now weakening

1701 UTC

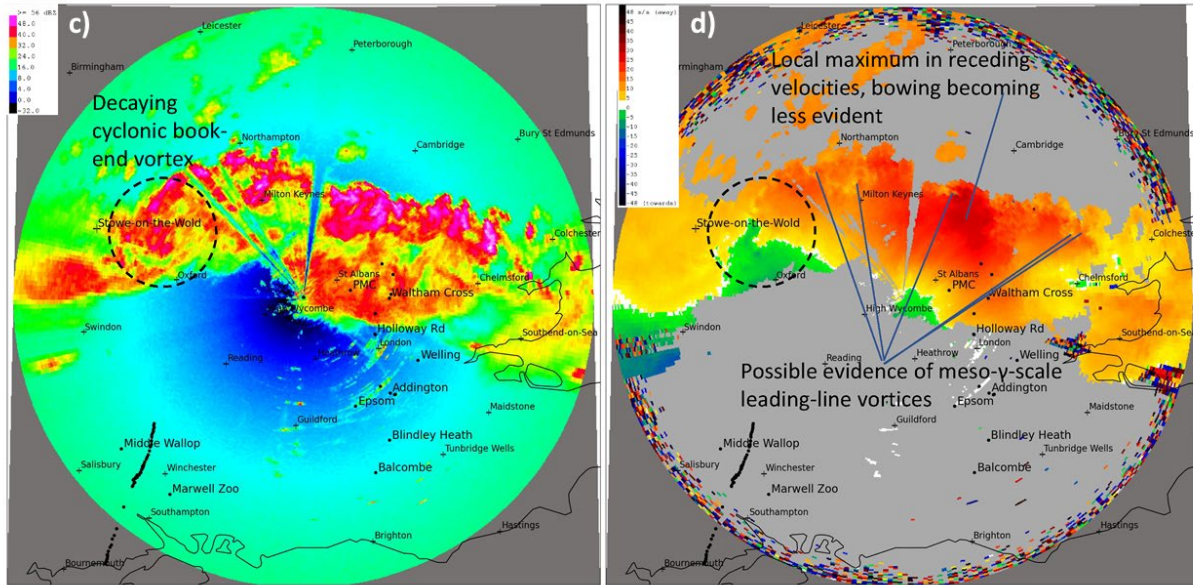


Figure 13. Chenies, UK radar reflectivity (left) and velocity (right) at 1631 UTC 23 October 2022. Black dots mark the location of reported damage.

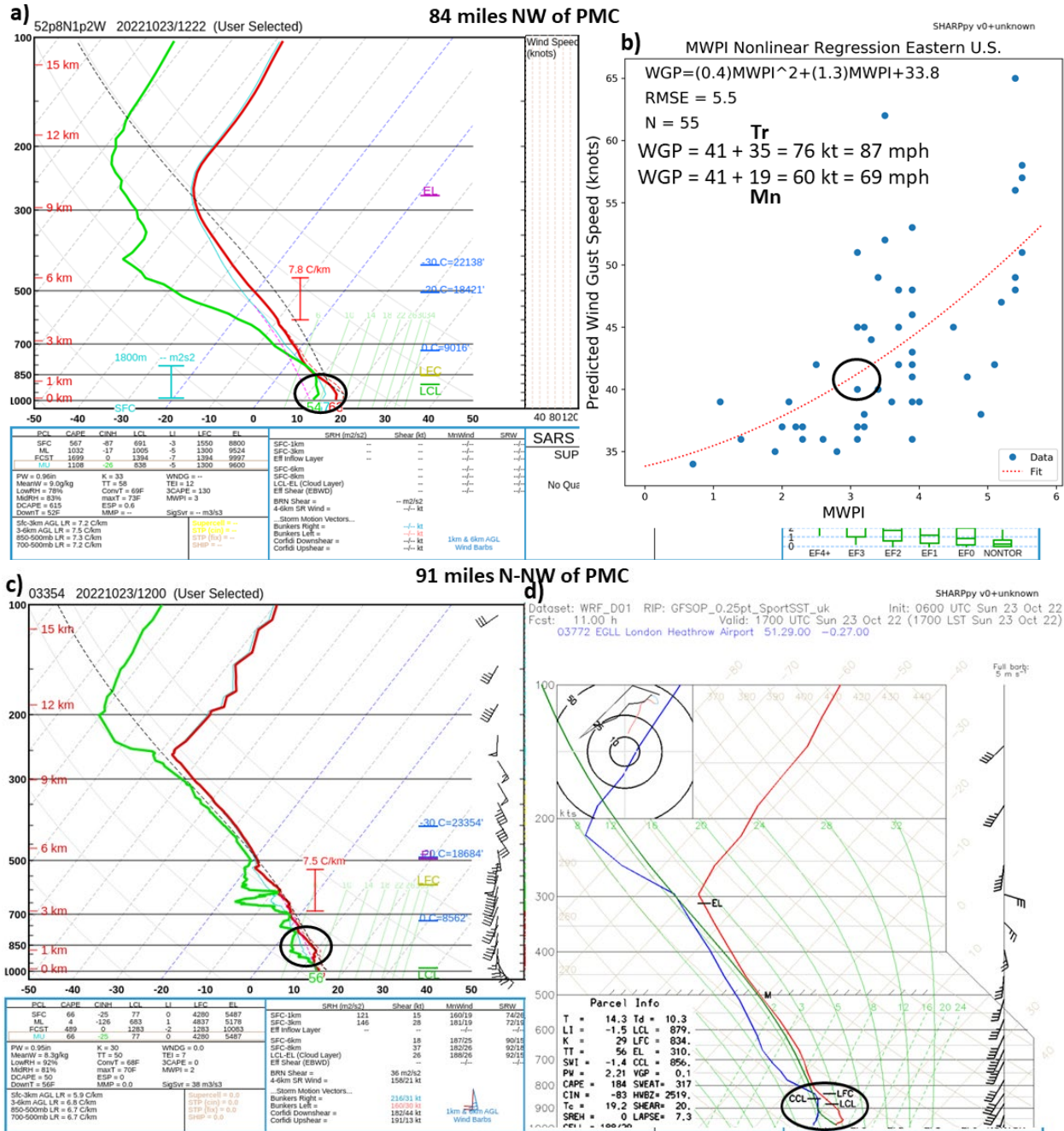


Figure 14. NUCAPS, WRF model, and RAOB sounding comparison: a) NUCAPS sounding profile over Loughborough, Leicestershire at 1222 UTC with the b) MWPI regression chart demonstrating the wind gust potential calculation technique; c) Nottingham RAOB profile at 1200 UTC, and d) WRF-model generated sounding profile over London Heathrow Airport at 1700 UTC 23 October 2022.

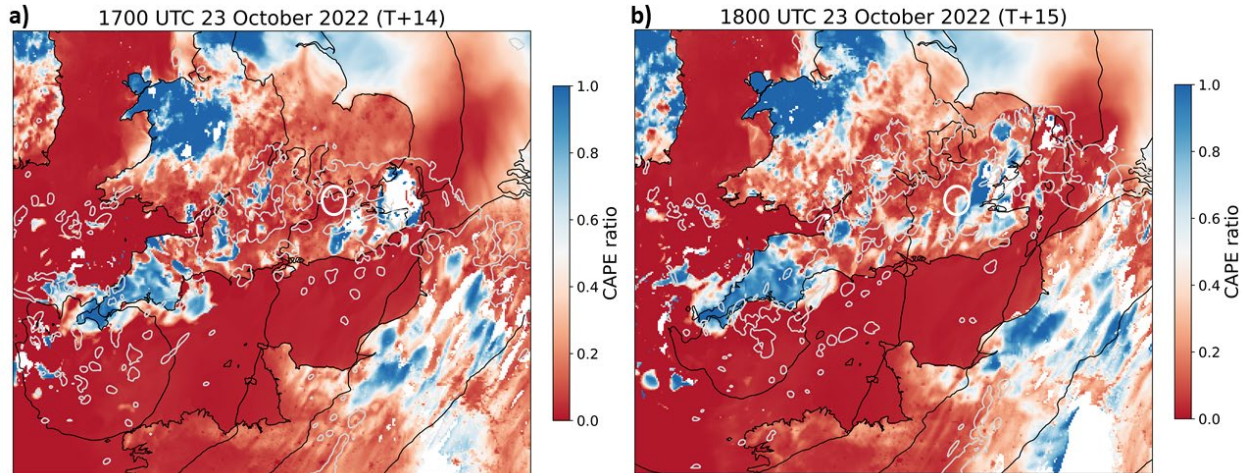


Figure 15. CAPE ratio diagnostic ( $1 - (\text{SBCAPE}/\text{MUCAPE})$ ) map from the UM forecasts of the 23 October 2022 QLCS: a) 1700 UTC and b) 1800 UTC. Reds indicate environments suitable for surface-based convection, blues indicate environments suitable for elevated convection. The gray contours show the 30 dBZ model reflectivity, and the black contours the MSLP. The white circle marks the location of downburst occurrence at London Colney, Hertfordshire.

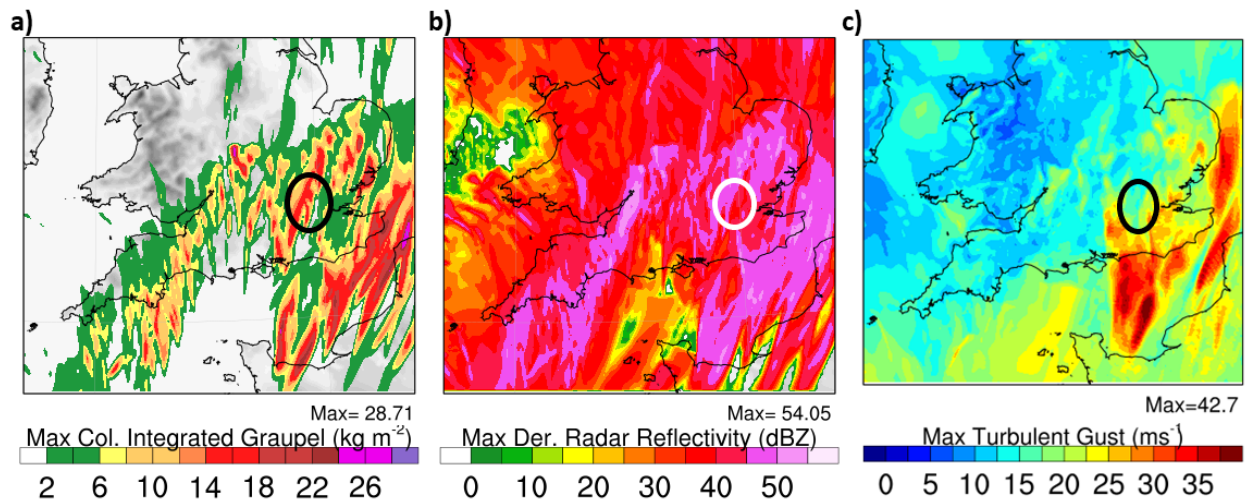


Figure 16. WRF model (UK3 D02)-derived convection diagnostic maps valid at 1800 UTC 23 October 2022: a) maximum column integrated graupel, b) maximum derived radar reflectivity, and c) maximum turbulent gust.